ACS APPLIED MATERIALS & INTERFACES

Research Article

Cite This: ACS Appl. Mater. Interfaces 2018, 10, 26765−26771

www.acsami.org

Alignment of Thermally Conducting Nanotubes Making High-Performance Light-Driving Motors

Meng Liao,[†] Hao Sun,[‡] Xin Tao,[§] Xiaojie Xu,[†] Zhi Li,[†] Xuemei Fu,[†] Songlin Xie,[†] Lei Ye,[†] Ye Zhang,[†] Bingjie Wang,[†] Xuemei Sun,[†] and Huisheng Peng*,[†]

[†]State Key Laboratory of Molecular Engineering of Polymers and Department of Macromolecular Science, Laboratory of Advanced Materials, and [§]Department of Materials Science, Fudan University, Shanghai 200438, China

[‡]Department of Chemistry, Stanford University, Stanford, California 94305, United States

Supporting Information

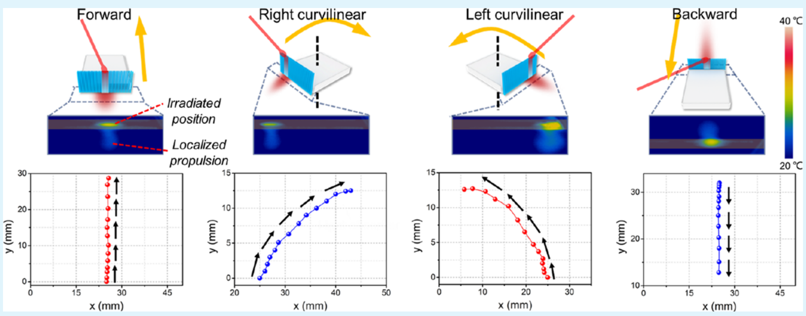

ABSTRACT: Light-actuating devices that can produce selective motions at small scales are highly desired for on-demand manipulation. For conventional photothermal motors that mostly encounter the homogenous light-induced heat diffusion at the liquid/air interface, it is challenging to effectively control the actuating direction and enhance the actuating speed. To this end, here, we explore aligned thermally conducting one-dimensional nanomaterials to make light-driving motors where the light-induced heat can be transmitted to the water surface along the length direction of the aligned one-dimensional nanomaterials to generate a localized surface tension gradient for high spatial resolution propulsion. When multiwalled carbon nanotubes were studied as a demonstration, the aligned active layer generated sufficient propulsion to drive a centimeter-sized motor that was 10 000 times higher in mass of the actuating layer on water. In addition, the actuating direction had been accurately controlled by varying the illuminated region of the active aligned nanotube layer. The resulting light-driving motors can move as fast as 4.19 cm/s (or 5.2 body length per second), which exceeded the previous motors based on the light activation.

KEYWORDS: *carbon nanotube, aligned, photo-thermal effect, light-driving, motor*

■ INTRODUCTION

The design and fabrication of actuating devices that can perform selective motions and tasks at small scales have attracted increasing interests at a variety of fields like robotics, microelectronics, environmental science, and biomedical engineering because of their promising advantages such as light weight, accurate control, and rapid response.[1−10] Among various driving strategies, the use of light to activate and control the small actuating devices had been intensively investigated because light is a clean, sustainable energy source, and it can be remotely and safely operated with high efficiency and low cost.[11−17] On the one hand, photoresponsive materials had been synthesized to directly convert light energy to mechanical energy, but they were limited to a low portion of functional organic materials,[18−20] and the repeatability was relatively poor particularly after a long irradiation because of the low stability of the organic systems. On the other hand, the small actuating devices can be driven through the use of a variety of inorganic materials based on a photothermal effect,[21−25] that is, the light was firstly converted to thermal energy and then to mechanical energy to offer the driving force. As a creative attempt, a photothermal layer was designed to convert light into heat at a liquid/solid interface, and the formed asymmetric thermal surface tension gradient was produced to push the resulting actuator to move on the liquid.[21] During the photothermal conversion process, the heat diffused throughout light absorbers into the whole neighboring liquid surface almost homogenously. Consequently, the photothermal utilization is low, and it remains challenging to accurately control the actuating direction and further enhance the actuating speed, which are required for various application fields such as microrobots.

In this work, we report a general and efficient strategy to make light-driving motors with accurately controlled actuating

Received: May 8, 2018
Accepted: July 12, 2018
Published: July 12, 2018

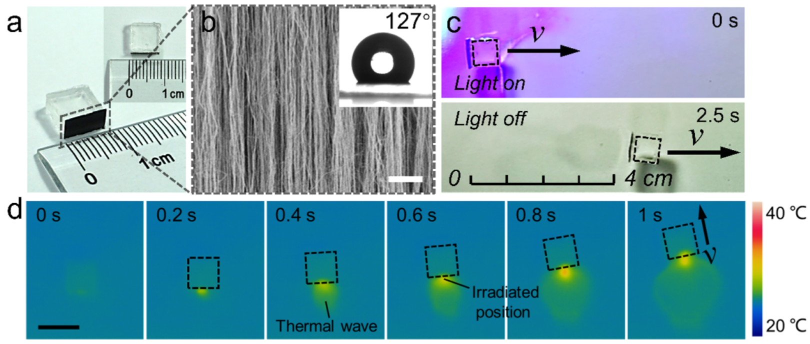

Figure 1. (a) Photographs of a vertically aligned MWCNT film-based light-driving motor. (b) SEM image of vertically aligned MWCNTs (inserted, the water contact angle of the surface). Scale bar, 10 μm. (c) Optical images of a motor in (a) by top view, recording a linear motion through the water surface when irradiated at the rear MWCNT side. (d) Thermal mapping images of the movement of the light-driving motor at different time points. The irradiation started at ~0 s. Scale bar, 1 cm.

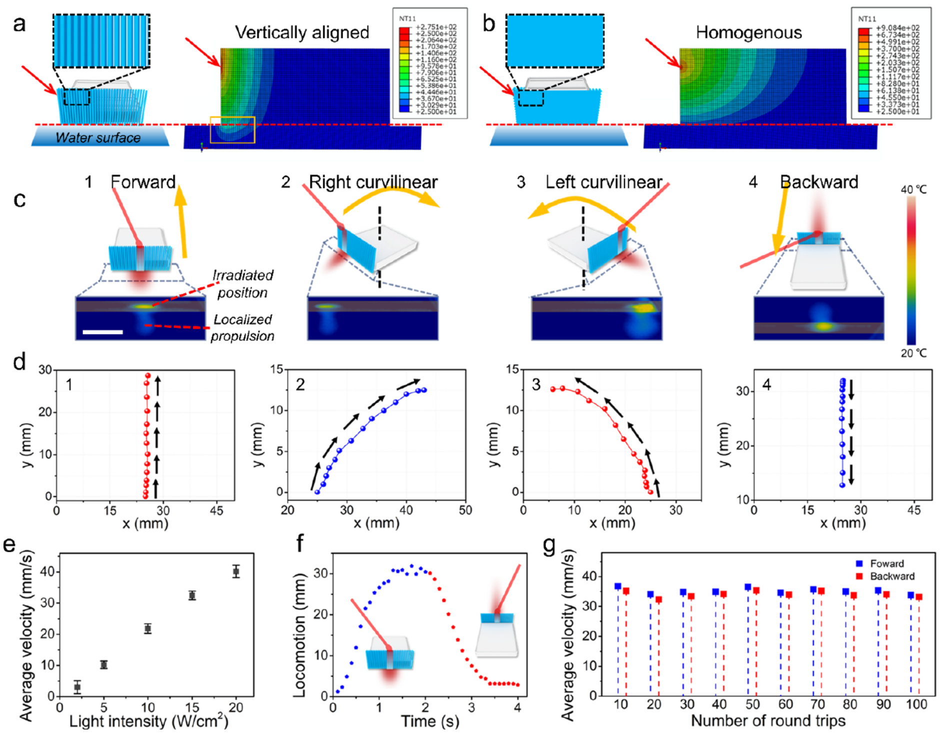

Figure 2. (a) Simulated thermal distribution of the light-activated motor based on the vertically aligned photothermal material and its neighboring water surface, with irradiation point at the leftmost side marked with a red arrow (irradiation for 1 s). Mediated with the vertical alignment, a hot zone right down the irradiated position was generated. (b) Simulated thermal distribution for the motor based on the homogenous photothermal material, with the other conditions to be the same as those of (a). The light-induced heat was uniformly spread from the irradiated site, and no hot zone was formed on the neighboring water surface. (c) Top panel, Schematic illustrations to the motors moving toward different directions manipulated by adjusting irradiated positions. Bottom panel, Thermal mappings recording the water surface and the vertically aligned MWCNT film above it when irradiated at different regions. The hot zone ejected from the motor rear can be interpreted as localized propulsion induced by the light. Scale bar, 2 mm. (d) Characteristic locomotion plots for typical controlled trails extracted from the videos. (e) Dependence of the mobility on the light intensity. (f) Typical forward and backward locomotion plots for vertically aligned MWCNT film-based motor under constant laser illumination. (g) Repeatability of reverse directional motions of the motor. Red and blue plots represented the average velocities of forward and backward motions, respectively.

directions and much improved moving speeds through the alignment of thermally conducting one-dimensional nanomaterials. Multiwalled carbon nanotubes (MWCNTs) had been here investigated as a demonstration for the high performance of this designing strategy. Our light-driving strategy demonstrates intriguing advantages including: (i) it combines efficient light collection and utilization in one material, delivering enhanced mobility up to 4.19 cm/s (or 5.2 body length per second); (ii) the rationally designed aligned nanostructure can regulate and control the navigating trail with high spatial resolution; and (iii) it introduces no chemical intermediate to the actuating system and thus concurrently enables high stability and repeatability.

RESULTS AND DISCUSSION

To fabricate a light-driving motor, the aligned MWCNT film that had been dry-drawn from a spinnable MWCNT array was attached onto a polydimethylsiloxane (PDMS) substrate

DOI: 10.1021/acsami.8b07499
ACS Appl. Mater. Interfaces 2018, 10, 26765−26771

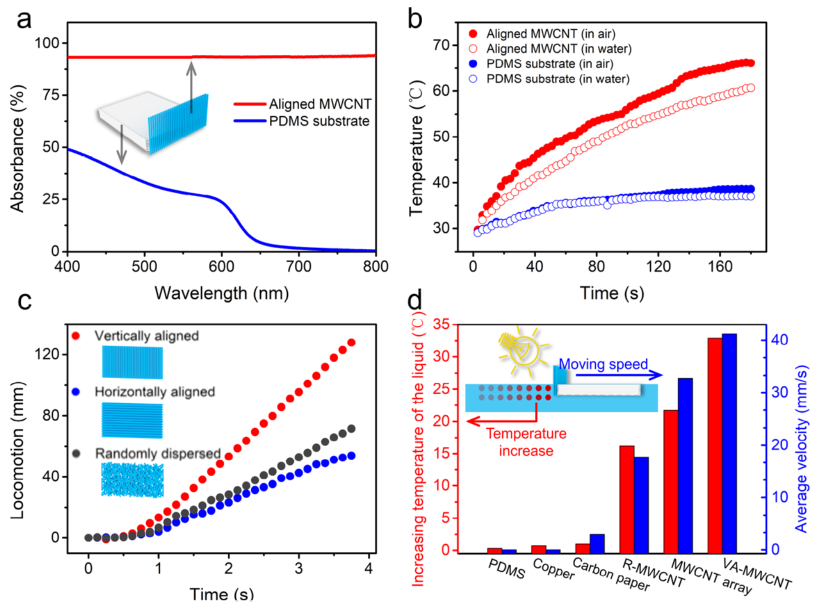

Figure 3. (a) Absorption spectra of the aligned MWCNT (light-activated layer of the motor) and the PDMS (motor substrate). (b) Dependence of the surface temperature on the irradiation time for the aligned MWCNT and the PDMS substrate measured in air and in water, respectively. (c) Locomotion plots from motors based on MWCNT networks with different aligned directions. (d) Relationships between the heating difference and obtained average velocity of light-driving motors incorporated with six different representative materials as light absorbers. Red bars, surface temperature variations induced by a constant illumination at the motors based on PDMS, copper, carbon paper, randomly dispersed MWCNT (R-MWCNT), MWCNT array, and vertically aligned MWCNT film (VA-MWCNT). Blue bars, average velocities of the above motors.

cuboid (Figure 1a). The MWCNTs were vertically aligned on the water surface (Figure 1b), and the aligned structures were well maintained after immersion in water for 24 h (Figure S1). If not otherwise specified, a thickness of ∼800 nm was generally utilized in this work. The MWCNT film was hydrophobic with a static contact angle of 127° (Figure 1b, inserted). This feature benefited the effective motion because the hydrophobicity lowered the water resistance for motors to move on the water surface.

When subjected to the concentrated light, the absorption[26] and the photothermal conversion[27] occurred in MWCNTs, and the temperature of MWCNT film dramatically increased, followed by a rapid thermal transmission to the surrounding liquid surface along the vertically aligned MWCNTs. The heated liquid surface at the rear of the motor delivered a relatively higher surface tension than that of the surrounding, unheated liquid surface. Because a liquid with relatively high surface tension pulls more strongly on the surrounding liquid than one with a low surface tension, the thermal surface tension gradient will naturally cause the liquid to flow away from regions of low surface tension, pushing the motor forward (Figure 1c and Movie S1).[21,25,28] Once the motor passed this location, the heated surface restored to its original state by the ambient air, and no intermediate was introduced to the whole motor system (Figure S2). In our work, an aligned MWCNT film with an area of ∼8 mm^2 can generate sufficient propulsion to drive a centimeter-sized motor up to ∼10 000 times higher in mass (a cuboid with volume of ∼2.3 cm^3) of the actuating layer on water (Figure S3). To investigate the photothermal propulsion, the light-activated movement was recorded by an infrared camera using frame-by-frame analysis (Figure 1d and Movie S2). The thermal wave, representing the high-temperature profile along the moving direction, continuously extended with the increasing irradiation time. The highest temperature appeared at the rear part of the motor after illuminating at a certain position. Such thermal waves were similar to photothermal induced hot vapor jet flow in the recent report,[23] which were ejected backward from the center hot zone on the motor rear and pushed the motor forward for enhanced mobility. As a comparison, the light irradiation on a bare PDMS cuboid turned out to be no response (Figure S4).

To accurately manipulate the light-activated motions on water, it is essential to convert light into gradient propulsion in a highly localized manner and directionally push the motor. However, in previously reported light-driving systems based on photothermal mechanisms, when the motors were exposed to light, the light-induced heat diffused throughout homogenous light absorbers, and then the thermal surface tension gradient spread to the whole neighboring liquid surface, mostly resulting in ill-controlled motions.[13] In this work, undesired thermal diffusion was effectively restricted because the thermal conductivity along the vertically aligned direction far surpassed that of the other direction.[29] Herein, highly localized propulsion was produced from selective light-irradiated positions, thus leading to a manipulation with better spatial resolution. For illustration, the heat transmission properties of two kinds of motors based on vertically aligned and homogenous photothermal materials (taking MWCNT networks as models) were studied through a finite element analysis simulation (Figure 2a,b and Movie S3). After irradiation by the same light beam at the leftmost sides (marked with red arrows in Figure 2a,b) for 1 s, the vertically aligned light absorber transferred heat to the surrounding liquid surface mainly along the vertically aligned direction and produced a narrower hot zone (marked with a yellow box in Figure 2a) right down the irradiated position, which can be interpreted as a precise conversion from input light signal to output propulsion. Thus, in comparison with homogenous light absorbers (Figure 2b), the vertically aligned photothermal

DOI: 10.1021/acsami.8b07499
ACS Appl. Mater. Interfaces 2018, 10, 26765−26771

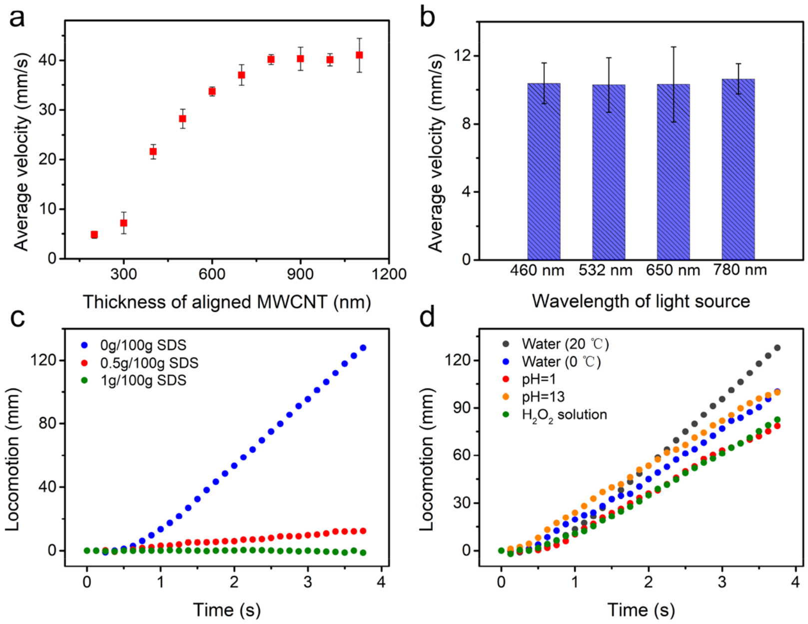

Figure 4. (a) Dependence of the mobility on the thickness of the aligned MWCNT film. (b) Dependence of the mobility on the wavelength of the driving light source. (c) Locomotion plots for light-driving motors with different surface tensions mediated by surfactant (SDS). Motion curves depict the quenching effect of this driving mechanism. (d) Locomotion plots for light-driving motors in varying aqueous liquid environments.

materials can produce highly localized propulsions for controllable motions.

The light beam was applied on the central, left, and right regions of the vertically aligned MWCNT film on the motor for a direct observation (Movie S4), and infrared images were recorded for the MWCNT film above the water and the water surface from the top view. The light-induced hot zones were ejected from the irradiated sites, generating propulsions ahead, toward right front, and toward left front (Figures 2c and S5). The corresponding motion curves were traced by a high-speed camera and further re-constructed through a frame-by-frame analysis (Figure 2d). For a curvilinear motion, a turning radius of 16 mm was achieved (Figure 2d2), verifying the controllability of a high spatial resolution. Here, the free-standing vertically aligned MWCNTs were prepared with a height over the PDMS cuboid, and the light-activated response can be thus produced under illumination on the back side of the film (Figure 2c4), producing a backward linear trail (Figure 2d4). The temperature change of the motor rear (aligned MWCNT) increased from 32.7 to 92.6 °C with increasing applied light intensity from 2 to 20 W/cm^2 (Figure S6). In addition, the speed of the motor could be controlled from 3.04 to 40.16 mm/s by tuning light intensity (Figure 2e), allowing the fabrication of more sophisticated light-manipulated systems. As a noninvasive, light-manipulated strategy, this motor system demonstrated desirable repeatability. For instance, the motor could be steered to produce reverse directional motions, that is, moving forward and then backward over a distance of ~60 mm in each trip, for 100 cycles (Figure 2f) without obvious velocity decay (Figure 2g).

Under the premise that motions could be controlled, high photothermal performance of the MWCNT light absorber and the vertical alignment of thermally conducting nanotubes also contributed to an improved mobility for light-driving motors. As the light absorber in this work, the aligned MWCNT film exhibited a high absorption capacity (>93%) of wavelengths from 400 to 800 nm (Figure 3a). By contrast, the PDMS substrate was almost transparent at this wavelength range, which benefited a focused absorption on the light-activated MWCNT layer for improved light utilization. To evaluate the photothermal property, the time-independent temperature variations of the aligned MWCNT and the PDMS substrate were monitored both in air and in water. After irradiation for 180 s (500 mW/cm^2) in air, the temperature of the aligned MWCNT surged from 29.5 to 66.12 °C (Figure 3b), which far exceeded that of the PDMS. The temperature increases in water shared the same trend and was slightly lower than that in air. Therefore, high efficient photothermal conversion of aligned MWCNT could lead to a huge temperature difference along the anterior−posterior axis (between PDMS substrate and MWCNT layer). This was key to enhance the mobility because the increasing temperature difference would produce amplified surface tension gradient, thus providing a strengthened propulsion according to the Harkins formula[22]

$$\gamma = b_0 + b_1T + b_2T^2$$

where γ is the local surface tension, T is temperature (°C), b_0 (75.796 mN/m), and both b_1 [−0.145 mN/(m·°C)] and b_2 [−0.00024 mN/(m·°C^2)] are constants.

We further studied the influence of MWCNT-aligned directions on the obtained velocity of corresponding light-driving motors (Figure 3c). As expected, the motor based on vertically aligned MWCNTs to water surface showed higher moving speed (>30 mm/s) over those of motors based on horizontally aligned and randomly dispersed MWCNTs. This could be explained by the fact that the vertical alignment of the thermally conducting MWCNTs favored a more direct thermal transmission to the water surface because the light-induced thermal transmission occurred mainly along the MWCNT alignment. Meanwhile, the aligned nanostructure regulating thermal transmission also contributed to a quick response to establish the light-induced temperature gradient for propulsion. For instance, irradiated by the same light source (100 mW/cm^2), a temperature variation of ~20 °C was achieved

DOI: 10.1021/acsami.8b07499
ACS Appl. Mater. Interfaces 2018, 10, 26765−26771

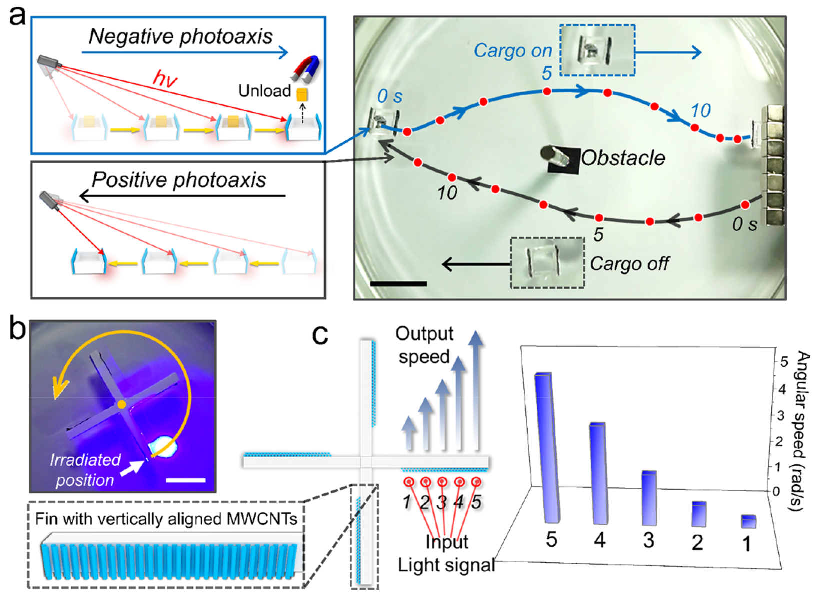

Figure 5. (a) Light-steered manipulation of the transport boat through an obstacle course. An iron cargo placed on the boat was carried and sent to the rightmost magnetic holder through a curvilinear ship line winding over the obstacle (following the blue line). After unloading, the boat was called back in following the positive photoaxis (following the black line). The final location of the transport boat was superimposed upon the original image. Scale, 2 cm. (b) Photograph showing the rotation of a speed-tunable floating rotor. Vertically aligned MWCNTs were incorporated to clockwise side of rotor fins. Scale bar, 2 cm. (c) Scheme illustrating the variation of angular speed of the rotor obtained by tuning the irradiating site.

within 20 s along the aligned direction of the MWCNT film, whereas it needed more than 40 s to establish the temperature gradient along the other directions (details in Note S3, Figures S7, and S8). In practical motor propulsion (driven by a laser of 20 W/cm^2), the light-driving motor exhibited a quick response within 0.2 s and established the temperature gradient in ~2 s, then achieving a maximal speed of 4.19 cm/s (Movie S2). To further evaluate the improved mobility from our design of both desirable light absorption and thermal transmission, we fabricated and tested a series of motors based on six representative materials, that is, bare PDMS (motor substrate), copper (high thermal conductivity while poor light absorption), commercial carbon paper (high light absorption while poor thermal conductivity), randomly dispersed MWCNT, and MWCNT array (Figure S9). First, the vertically aligned MWCNT outperformed the other materials in the capacity of the photothermal conversion for propulsion, which enacted as the most drastic light-induced temperature difference by 49.7 °C under a constant illumination for 10 s (light intensity, 10 W/cm^2, Figure 3d). Second, the floating motor made from the vertically aligned MWCNT film also demonstrated a higher velocity over that of the other contrast material.

The dependence of the motor performance on several key parameters had been systematically investigated by a number of control experiments. First, when a motor was driven on a water surface (light intensity of 20 W/cm^2) with increasing MWCNT thicknesses from 200 to 800 nm, the average moving speed increased from 0 to 40.16 mm/s (Figure 4a). No obvious enhancement of moving speed was observed when further increasing the thickness to 1 μm (~50 layers of stacked aligned MWCNT sheets). Second, motors driven by a light source (~5 W/cm^2) of various wavelengths, that is, 460 nm (blue), 532 nm (green), 650 nm (red), and 780 nm (near infrared ray, NIR) delivered effective motions with average velocities of 10.41, 10.29, 10.32, and 10.65 mm/s, respectively (Figure 4b). Although the NIR laser induced a relatively higher moving speed, its invisibility made inconvenience for real-time control. It should be noted that by using a light absorber with wavelength-selective absorption properties, a more sophisticated and programmable light-triggered actuating system may be achieved.[30] Third, the light-driven motion was quenched with the addition of surfactant (sodium dodecyl sulfate, SDS) on the water surface (Figure 4c) because it cuts surface tension effects. Finally, the light-induced propulsion was also effective under various aqueous environmental conditions that tend to deactivate most chemical fuel-driving motors, such as extreme pH values (i.e., pH = 1 and pH = 14), strong oxidizability, and low temperature of 0 °C (Figure 4d). Apart from the aqueous solution, the light-driving motor could also move in a spectrum of organic solvents (Figure S10) including isopropyl alcohol and dimethyl formamide, suggesting its environmental adaptability with desirable controllability.

These novel light-driving motors showed promising applications in a spectrum of fields. A light-manipulated transport ship was here assembled to demonstrate the capability of on-demand motions by swimming through an obstacle course (Figure 5a). The prototype was fabricated by incorporating two pieces of vertically aligned MWCNT films into the opposite sides of a PDMS cuboid containing a cavity for cargo loading (Figure S11). An iron foil (~0.5 g) was placed on the boat as a cargo, and the boat was steered to the targeted spot along a curved trail by alternating linear motion and turning maneuvers at an average speed of 9.7 mm/s (Movie S5). After unloading the iron cargo by a magnetic holder, the boat was called back along a curvilinear trajectory, winding over the obstacle in a swift manner again. The same boat was also manipulated to navigate around in a mini-circle (diameter of ~8.2 mm), suggesting its high spatial solution for more complicated motions.

Benefiting from the high motion controllability and device simplicity, the light-driving motors could be further used as building blocks to assemble into complicated and tunable

DOI: 10.1021/acsami.8b07499
ACS Appl. Mater. Interfaces 2018, 10, 26765−26771

systems to better meet the application requirements (e.g., macroscopic supramolecular assembly,[31] surface chemistry, and oil collection) under the guidance of light (Figure S12 and Movie S6), demonstrating the potential for collaborative behavior among individual microrobots in the future. Moreover, it was also efficient to assemble them into actuating systems for rotatory movements. For instance, four vertically aligned MWCNT films were placed on the clockwise face of each fin of a rotor (Figure 5b), and the rotations (Movie S7) could be controlled to produce tunable output angular speeds from 0.32 to 5.3 rad/s by shifting the input irradiated sites (from 1 to 5) on the rotor (Figure 5c).

CONCLUSION

In summary, different from the conventional light-driving motors that are generally fabricated from homogenous light absorbers, here, we have developed a series of new light-driving motors with high performances by aligning thermally conducting one-dimensional nanomaterials as the active layer. The resulting light-driving motors displayed both high direction controllability and moving speed. This work represents a general and promising strategy in the development of stimuli-responding motors with high properties.

EXPERIMENTAL SECTION

Light-Driving Motor Production. The aligned MWCNT film was paved onto a transparent quartz slice (8×6 mm^2, thickness of ~0.05 mm), and then the composite film was adhered to the rear of a PDMS cuboid ($8 \times 8 \times 4$ mm^3). The substrate cuboid was prepared by curing PDMS (Ecoflex 30, Smooth-On, USA) at a temperature of 80 °C for 3 h. The density of the as-prepared PDMS cuboid was 1.16 g/cm^3. The transparent PDMS and ultrathin quartz slice contributed to a more focused absorption of light on the aligned MWCNT film.

Speed-Tunable Rotor Production. Polyvinyl chloride foam plate (thickness of 4 mm, density of 0.38 g/cm^3) was cut into a cross shape. The length and width of each fin were 2.5 and 0.4 cm, respectively. Four pieces of aligned MWCNT films (4×15 mm^2) were placed on the clockwise face of each fin to form the light-driving rotor (Figure 5b). The MWCNT-covered area was further divided into five uniform parts (Figure 5c). Applying light beam on the above five parts generated angular speeds of the rotor from 0.32 to 5.3 rad/s.

Motor Testing. Light-induced heating and liquid/air interfacial motion were tested and quantified by applying laser irradiation at the rear (aligned MWCNT film) of the motor. The heat transmission of the liquid surface was recorded by an infrared camera, and the average temperature variation on the liquid was extracted for quantification and calculation. The moving trail was shot by a digital camera. By measuring the length of the normal graph paper under motors, the passing distance and the velocity were extracted through video image analysis.

Simulation of the Thermal Transmission. The simulation mainly focused on the thermal transmission on the light-activated layer and the resulted temperature variation on water surface. The model was built with finite element software Abaqus. In the model, light beam (diameter of 1 mm, 15 W/cm^2) was applied at the vertically aligned MWCNT film. The light-induced heat transmitted to the neighboring water surface. The areas of two MWCNT-based films were 8×4 mm^2, and the thickness of heated water layer was 0.5 mm. The ambient temperature was 25 °C. $\rho_{\mathrm{MWCNT}} = 454.57$ kg/m^3. $\rho_{\mathrm{H_2O}} = 1000$ kg/m^3. The thermal conductivities of vertically aligned MWCNTs (along the aligned direction), isotropic MWCNT array, and water surface were 3000, 200, and 0.6 W/mK,[28] respectively. The specific heat capacities of MWCNTs and water were 470 and 4200 J/(kg·K), respectively. The coefficients of heat dispersion for air and water were 20 and 100, respectively. The same parameters were applied to homogenous MWCNT networks for simulation in Figure 2b.

Light-Driving Locomotion for Assembling Motor Building Blocks. Building blocks (PDMS cuboid with a cavity in the center) were fabricated according to the same process in Figure S11. The surfaces of PDMS films were hydrophobic. Two pieces of hydrophilic aligned MWCNT films were produced through the treatment with an oxygen microwave plasma under an oxygen gas flow rate of 300 sccm and a power of 300 W (Plasma System 690, PVA Tepla) from pristine aligned MWCNT films. The treatment time was varied from 5 to 40 min to tune the degree of hydrophilicity. The hydrophobic PDMS/hydrophilic MWCNT composite cuboids were manipulated under the guidance of light and assembled together because of the minimizing interfacial free energy.

Characterization. To activate the light-driving motor and achieve enhanced mobility, a highly localized, point source light of high intensity was needed. Herein, a blue laser generator with a wavelength of 460 nm, powering density of 20 W/cm^2, and typical laser beam of ~1 mm in diameter was used to produce and manipulate the liquid/air interfacial surface. The powering density of the laser was tuned from 2 to 20 W/cm^2 by optical filters in control experiments. For the convenience of thermal conducing observation and accurate record, area light sources of relatively low intensity (e.g., 500 and 100 mW/cm^2) were employed in related control experiments (Figures 3a and S8). In this case, the visible light was generated by a solar simulator with AM1.5 solar light (Lansheng XQ350W, Shanghai, equipped with a 350 W Xe lamp and an AM1.5 filter-typical solar spectrum). The microstructures of aligned MWCNT films and MWCNT array were characterized by scanning electron microscopy (SEM, Hitachi FE-SEM S-4800 operated at 1 kV). For absorption spectra testing, 40 layers of aligned MWCNT sheets were paved and stacked on a quartz plate. The absorption spectra were obtained from an ultraviolet and visible spectrophotometer (Lambda 750). All of the thermal properties and images were obtained from an infrared camera (PI 450, Optris). Average temperature variations of liquid surfaces during motion were measured throughout the work. Photographs were captured by a camera (A5000, Sony).

ASSOCIATED CONTENT

Supporting Information

The Supporting Information is available free of charge on the ACS Publications website at DOI: 10.1021/acsami.8b07499.

Details of preparation process of aligned MWCNT films, photothermal conversion of aligned MWCNT and PDMS films, experimental results of aligned nanostructure regulating thermal transmission, Figures S1–S12, and Movies S1–S7 (PDF)

Linear motion through the water surface of a light-driving motor when irradiated at the rear MWCNT side (ZIP)

Thermal mapping video of a moving light-driving motor (ZIP)

Simulated thermal distribution of the light-activated motor based on vertically aligned MWCNTs and its neighboring water surface (ZIP)

Directional motions manipulated by varying irradiating sites (ZIP)

Light-steered transport boat through an obstacle course (ZIP)

Light-driving macroscopic assembly (ZIP)

Light-driving rotor (ZIP)

AUTHOR INFORMATION

Corresponding Author

*E-mail: penghs@fudan.edu.cn.

ORCID

Huisheng Peng: 0000-0003-3746-8494

Author Contributions

The manuscript was written through contributions of all the authors. All the authors have given approval to the final version of the manuscript.

Notes

The authors declare no competing financial interest.

■ ACKNOWLEDGMENTS

This work was supported by Ministry of Science and Technology of China (2016YFA0203302), National Natural Science Foundation of China (21634003, 51573027, 51403038, 51673043, 21604012) and Science and Technology Commission of Shanghai Municipality (16JC1400702, 15XD1500400, 15JC1490200).

■ REFERENCES

(1) Tu, Y.; Peng, F.; Wilson, D. A. Motion Manipulation of Micro- and Nanomotors. *Adv. Mater.* **2017**, *29*, 1701970−1701989.

(2) Hu, W.; Lum, G. Z.; Mastrangeli, M.; Sitti, M. Small-Scale Soft-Bodied Robot with Multimodal Locomotion. *Nature* **2018**, *554*, 81−85.

(3) Chang, S. T.; Paunov, V. N.; Petsev, D. N.; Velev, O. D. Remotely Powered Self-Propelling Particles and Micropumps based on Miniature Diodes. *Nat. Mater.* **2007**, *6*, 235−240.

(4) Zhang, J.; Song, L.; Zhang, Z.; Chen, N.; Qu, L. Environmentally Responsive Graphene Systems. *Small* **2014**, *10*, 2151−2164.

(5) Loget, G.; Kuhn, A. Electric Field-Induced Chemical Locomotion of Conducting Objects. *Nat. Commun.* **2011**, *2*, 535.

(6) Ismagilov, R. F.; Schwartz, A.; Bowden, N.; Whitesides, G. M. Autonomous Movement and Self-Assembly. *Angew. Chem., Int. Ed.* **2002**, *41*, 652−654.

(7) Jin, H.; Marmur, A.; Ikkala, O.; Ras, R. H. A. Vapour-Driven Marangoni Propulsion: Continuous, Prolonged and Tunable Motion. *Chem. Sci.* **2012**, *3*, 2526−2529.

(8) Park, J. H.; Lach, S.; Polev, K.; Granick, S.; Grzybowski, B. A. Metal-Organic Framework "Swimmers" with Energy-Efficient Autonomous Motility. *ACS Nano* **2017**, *11*, 10914−10923.

(9) Zhang, H.; Duan, W.; Liu, L.; Sen, A. Depolymerization-Powered Autonomous Motors Using Biocompatible Fuel. *J. Am. Chem. Soc.* **2013**, *135*, 15734−15737.

(10) Mou, F.; Chen, C.; Ma, H.; Yin, Y.; Wu, Q.; Guan, J. Self-Propelled Micromotors Driven by the Magnesium-Water Reaction and their Hemolytic Properties. *Angew. Chem., Int. Ed.* **2013**, *52*, 7208−7212.

(11) Xu, L.; Mou, F.; Gong, H.; Luo, M.; Guan, J. Light-driven Micro/Nanomotors: from Fundamentals to Applications. *Chem. Soc. Rev.* **2017**, *46*, 6905−6926.

(12) Hu, Y.; Li, Z.; Lan, T.; Chen, W. Photoactuators for Direct Optical-to-Mechanical Energy Conversion: From Nanocomponent Assembly to Macroscopic Deformation. *Adv. Mater.* **2016**, *28*, 10548−10556.

(13) Chen, X.-Z.; Jang, B.; Ahmed, D.; Hu, C.; De Marco, C.; Hoop, M.; Mushtaq, F.; Nelson, B. J.; Pané, S. Small-Scale Machines Driven by External Power Sources. *Adv. Mater.* **2018**, *30*, 1705061−1705082.

(14) Chen, C.; Mou, F.; Xu, L.; Wang, S.; Guan, J.; Feng, Z.; Wang, Q.; Kong, L.; Li, W.; Wang, J. Light-Steered Isotropic Semiconductor Micromotors. *Adv. Mater.* **2017**, *29*, 1603374−1603381.

(15) Liu, M.; Zentgraf, T.; Liu, Y.; Bartal, G.; Zhang, X. Light-Driven Nanoscale Plasmonic Motors. *Nat. Nanotechnol.* **2010**, *5*, 570−573.

(16) Dai, B.; Wang, J.; Xiong, Z.; Zhan, X.; Dai, W.; Li, C.-C.; Feng, S.-P.; Tang, J. Programmable Artificial Phototactic Microswimmer. *Nat. Nanotechnol.* **2016**, *11*, 1087−1092.

(17) Wu, Z.; Si, T.; Gao, W.; Lin, X.; Wang, J.; He, Q. Superfast Near-Infrared Light-Driven Polymer Multilayer Rockets. *Small* **2016**, *12*, 577−582.

(18) Ercole, F.; Davis, T. P.; Evans, R. A. Photo-Responsive Systems and Biomaterials: Photochromic Polymers, Light-Triggered Self-Assembly, Surface Modification, Fluorescence Modulation and Beyond. *Polym. Chem.* **2010**, *1*, 37−54.

(19) Hosono, N.; Kajitani, T.; Fukushima, T.; Ito, K.; Sasaki, S.; Takata, M.; Aida, T. Large-Area Three-Dimensional Molecular Ordering of a Polymer Brush by One-Step Processing. *Science* **2010**, *330*, 808−811.

(20) Jiang, Z.; Xu, M.; Li, F.; Yu, Y. Red-Light-Controllable Liquid-Crystal Soft Actuators via Low-Power Excited Upconversion based on Triplet-Triplet Annihilation. *J. Am. Chem. Soc.* **2013**, *135*, 16446−16453.

(21) Okawa, D.; Pastine, S. J.; Zettl, A.; Fréchet, J. M. J. Surface Tension Mediated Conversion of Light to Work. *J. Am. Chem. Soc.* **2009**, *131*, 5396−5398.

(22) Wang, W.; Liu, Y.-Q.; Liu, Y.; Han, B.; Wang, H.; Han, D.-D.; Wang, J.-N.; Zhang, Y.-L.; Sun, H.-B. Direct Laser Writing of Superhydrophobic PDMS Elastomers for Controllable Manipulation via Marangoni Effect. *Adv. Funct. Mater.* **2017**, *27*, 1702946−1702953.

(23) Meng, F.; Hao, W.; Yu, S.; Feng, R.; Liu, Y.; Yu, F.; Tao, P.; Shang, W.; Wu, J.; Song, C. Vapor-Enabled Propulsion for Plasmonic Photothermal Motor at the Liquid/Air Interface. *J. Am. Chem. Soc.* **2017**, *139*, 12362−12365.

(24) Xuan, M.; Wu, Z.; Shao, J.; Dai, L.; Si, T.; He, Q. Near Infrared Light-Powered Janus Mesoporous Silica Nanoparticle Motors. *J. Am. Chem. Soc.* **2016**, *138*, 6492−6497.

(25) Maggi, C.; Saglimbeni, F.; Dipalo, M.; De Angelis, F.; Di Leonardo, R. Micromotors with Asymmetric Shape that Efficiently Convert Light into Work by Thermocapillary Effects. *Nat. Commun.* **2015**, *6*, 7855.

(26) Wang, T.; Torres, D.; Fernández, F. E.; Green, A. J.; Wang, C.; Sepúlveda, N. Increasing Efficiency, Speed, and Responsivity of Vanadium Dioxide Based Photothermally Driven Actuators Using Single-Wall Carbon Nanotube Thin-Films. *ACS Nano* **2015**, *9*, 4371−4378.

(27) Yang, Z.-P.; Ci, L.; Bur, J. A.; Lin, S.-Y.; Ajayan, P. M. Experimental Observation of an Extremely Dark Material Made by a Low-Density Nanotube Array. *Nano Lett.* **2008**, *8*, 446−451.

(28) Huang, H.; Zhu, G.; Zhang, Y. Effect of Marangoni Number on Thermocapillary Convection in a Liquid Bridge under Microgravity. *Int. J. Therm. Sci.* **2017**, *118*, 226−235.

(29) Yang, D. J.; Zhang, Q.; Chen, G.; Yoon, S. F.; Ahn, J.; Wang, S. G.; Zhou, Q.; Wang, Q.; Li, J. Q. Thermal Conductivity of Multiwalled Carbon Nanotubes. *Phys. Rev. B: Condens. Matter Mater. Phys.* **2002**, *66*, 165440.

(30) Wang, P.; Zhao, G.; Wang, Y.; Lu, Y. MnTiO3-driven low-temperature oxidative coupling of methane over TiO2-doped Mn2O3-Na2WO4/SiO2catalyst. *Sci. Adv.* **2017**, *3*, e1603180.

(31) Cheng, M.; Ju, G.; Zhang, Y.; Song, M.; Zhang, Y.; Shi, F. Supramolecular Assembly of Macroscopic Building Blocks Through Self-Propelled Locomotion by Dissipating Chemical Energy. *Small* **2014**, *10*, 3907−3911.

DOI: 10.1021/acsami.8b07499
ACS Appl. Mater. Interfaces 2018, 10, 26765−26771